Journal of Computational Physics 227 (2008) 9865–9884

Contents lists available at ScienceDirect

Journal of Computational Physics

journal homepage: www.elsevier.com/locate/jcp

Simulations of the 2.5D inviscid primitive equations in a limited domain

Qingshan Chen [a,b,*], Roger Temam [b], Joseph J. Tribbia [c]

[a] Department of Mathematics, Indiana University, 831 E 3rd Street, Bloomington, IN 47405, United States
[b] The Institute for Scientific Computing and Applied Mathematics, Indiana University, Bloomington, IN 47405, United States
[c] National Center for Atmospheric Research Boulder, Colorado, United States

ARTICLE INFO

Article history:
Received 14 April 2008
Received in revised form 1 August 2008
Accepted 4 August 2008
Available online 17 August 2008

MSC:
35L50
65M06
76B99
86A05

Keywords:
Nonviscous primitive equations
Limited domains
Boundary conditions
Transparent boundary conditions
Finite difference methods

ABSTRACT

The primitive equations (PEs) of the atmosphere and the oceans without viscosity are considered. These equations are not well-posed for any set of local boundary conditions. In space dimension 2.5 a set of nonlocal boundary conditions has been proposed in Chen et al. [Q. Chen, J. Laminie, A. Rousseau, R. Temam, J. Tribbia, A 2.5D Model for the equations of the ocean and the atmosphere, Anal. Appl. 5(3) (2007) 199–229]. The present article is aimed at testing the validity of these boundary conditions with physically relevant data. The issues tested are the well-posedness in the nonlinear case and the computational efficiency of the boundary conditions for limited area models [T.T. Warner, R.A. Peterson, R.E. Treadon, A tutorial on lateral boundary conditions as a basic and potentially serious limitation to regional numerical weather prediction, Bull. Amer. Meteor. Soc. 78(11) (1997) 2599–2617].

1. Introduction

This article is concerned with the primitive equations (PEs) without viscosity in space dimension 2.5, and is related to the more theoretical article [3].

When the viscosity is present, the primitive equations have been the object of much attention, on the mathematical side, since the works [9,10]; review articles about the mathematical theory of the PEs with viscosity appear in [22] and in an updated form in [16]; see also [2,7,8]. For the physical background on primitive equations, see e.g. [15] or [23].

In the absence of viscosity, little progress has been made on the analysis of the primitive equations since the negative result of Oliger and Sundstrom [14] showing that these equations are not well-posed for any set of local boundary conditions. However, the determination of suitable boundary conditions for the primitive equations is a very important problem for limited area models; see e.g. a discussion in [24].

In earlier works, two of the authors of the present article and A. Rousseau have investigated these equations in space dimension two, and an infinite set of boundary conditions has been proposed. Well-posedness of the corresponding linear-

* Corresponding author. Address: Department of Mathematics, Indiana University, 831 E 3rd Street, Bloomington, IN 47405, United States. Tel.: +1 812 855 4074; fax: +1 812 855 7850.
E-mail address: qinchen@indiana.edu (Q. Chen).

0021-9991/$ - see front matter © 2008 Elsevier Inc. All rights reserved.
doi:10.1016/j.jcp.2008.08.005

ized equations has been established in [18] and numerical simulations have been performed in [19] for the linearized equations and for the full nonlinear equations. Note that the nonoccurrence of blow-up in the latter case supports the (yet unproved) conjecture that the proposed nonlocal boundary conditions are also suitable for the nonlinear PEs. See also [1] for numerical issues concerning the boundary conditions for the primitive equations without viscosity.

The numerical simulations performed in [19] were mainly motivated by computational preoccupations and the need to support the idea that the proposed boundary conditions are computationally feasible and lead indeed to well-posedness. In view of performing (in dimension two) computations of physical significance, the last author expressed the wish that the flow should be a perturbation of a geostrophic flow (which is not the case in [19]). Now, the geostrophic equation

$$p_y = -\rho f u, \tag{1.1}$$

implies that there does not exist any geostrophic solution depending only on x and z.[1] It is then necessary, even in dimension two, to introduce some y-dependence. A number of natural choices had to be abandoned, in particular the use of a few Fourier modes in y, which would produce the undesirable Gibbs phenomena when approximating the periodic extension of the function $\sigma(y) = y$ on $[0, L_2]$, this function being introduced in the model by (1.1). In this way we were led to choose, for the y-direction, a three-mode linear finite element model. In the article [3], we presented the full derivation of the model and studied the well-posedness of the linearized equations.

The present article is aimed at actually testing in a physically relevant context the model in [3] which we here call a 2.5D model. In fact the model presented in [3] was a linear (linearized) one. The first step here is then to extend the model to the *nonlinear* case. Let us succinctly present the derivation of the model.

We first derive the Galerkin finite element approximation based on the use of three piecewise linear elements in the direction y; we thus arrive at three coupled systems, each one similar to the 2D primitive equations in the variables x and z (and t). We then perform the normal mode decomposition of these equations in the direction z as in [21] (see also [17–19]), the normal modes in z being either sines or cosines (depending on the functions), and these sines and cosines are the eigenfunctions of a two-point boundary value Sturm–Liouville problem ([21]). At this stage, each mode consists in three coupled equations for the functions of the variables x and t (Section 2.2). In Section 2.3, we recall the boundary conditions for the linearized systems in x and t, the boundary conditions depending on the nature of the mode (being the zero, or a subcritical or supercritical mode). The zero mode takes a special form and requires some special treatment, while the subcritical modes are the mathematically most challenging and physically most relevant ones. Finally, in Section 2.4, we introduce the boundary conditions for the nonlinear system derived above.

The numerical simulations are the focuses of the present article. In Section 3 the numerical schemes for the nonlinear systems are presented. We choose a first order finite difference method for the spatial discretization. However, care has to be taken of the signs of the characteristic values in order to take an upwind spatial discretization of the x-derivatives. For this reason the subcritical modes and the supercritical modes have to be treated differently (see Section 3.2). The zero mode is treated separately. For the time advancing we choose the first order semi-implicit finite difference method, i.e. the first order x-derivatives are treated implicitly (in time), while the zero order terms and the nonlinear terms are treated explicitly (in time).

The numerical simulations, as well as their results, are presented in Section 4. Two simulations are performed: the first one on a large domain, with homogeneous boundary conditions at one or both ends in the x-direction, and the second one on the middle half of the domain, with boundary data (usually nonhomogeneous) coming from the first simulation. The outcomes of both simulations are studied and compared. They support the conjecture that the proposed boundary conditions are suitable for the nonlinear problem. Both outcomes (restricted to the middle half domain if necessary) match very well on the middle half domain. This shows that the proposed boundary conditions are physically relevant. Let us recall here that the computational problem at the origin of this study is the choice of boundary conditions for limited area models based on the primitive equations. The similarity of the solutions computed with the parent (global) model and with the local one supports the idea that, beside being mathematically suitable, the nonlocal boundary conditions introduced in [3] for the 2.5D model are also computationally satisfactory for limited area simulations [24].

In a series of papers related to our articles, McDonald [11–13] studies the boundary conditions that are appropriate to the linearized Shallow Water equations, implements them in the context of a multi-level (nested) discretization and compares his numerical results to those given by the method of Davies [4]. The boundary conditions proposed by McDonald in [11] are based on the directions of the characteristics at the boundary and his point of view is close to ours (see the comments after (2.29) in the text). The method used by Davies is based on a relaxation of the boundary values of a given quantity u to its external values u_B given, e.g., by computations on a coarser mesh. This classical method introduces a boundary layer at the boundary which depends on the choice and our object, as well as that of the articles [11–13], is to avoid such boundary layers. See also [6] for a review and further discussions on the boundary conditions.

In this article, as well as in [3] and in our related articles, the Brunt–Väisälä frequency N of the underlying stratified flow is assumed to be constant (see below after (2.2)). Our results can be extended to more general positive frequencies $N = N(z)$, although some additional work would be needed in that case and the eigenfunctions $\mathcal{U}_n$ and $\mathcal{W}_n$ appearing in the normal

[1] Ox is the local west–east direction, Oy is the local south–north direction, and Oz is the ascendant vertical.

vertical expansion would be more complicated than the sines and cosines appearing in (2.14) below and they generally would not be known explicitly. These developments are left for further work.

2. The 2.5D primitive equations and their normal mode expansion

We recall that the 3D primitive equations without viscosity for the ocean and the atmosphere read:

$$\begin{cases} \tilde{\mathbf{v}}_t + (\tilde{\mathbf{v}}\cdot\nabla)\tilde{\mathbf{v}} + \tilde{w}\mathbf{v}_z + fk\times\tilde{\mathbf{v}} + \frac{1}{\rho_0}\nabla\tilde{p} = F_{\tilde{\mathbf{v}}}, \\ \tilde{p}_z = -\tilde{\rho}g, \\ \nabla\cdot\tilde{\mathbf{v}} + \tilde{w}_z = 0, \\ \tilde{T}_t + (\tilde{\mathbf{v}}\cdot\nabla)\tilde{T} + \tilde{w}\tilde{T}_z = Q_{\tilde{T}}, \\ \tilde{\rho} = \rho_0(1-\alpha(\tilde{T}-T_0)). \end{cases} \tag{2.1}$$

Here $\tilde{\mathbf{v}} = (\tilde{u},\tilde{v})$ is the horizontal velocity, $\tilde{w}$ the vertical velocity, $\tilde{\rho}$ is the density, $\tilde{p}$ the pressure, and $\tilde{T}$ the temperature; ∇ denotes the horizontal gradient operator; $\tilde{\mathbf{v}}_t = \partial\mathbf{v}/\partial t$, etc. The independent variables are $(x,y,z)\in\mathcal{M} = (0,L_1)\times(0,L_2)\times(-H,0)$, and $t>0$. The forcing terms $F_{\tilde{\mathbf{v}}} = (F_{\tilde{u}},F_{\tilde{v}})$ and $Q_{\tilde{T}}$ are introduced here merely for mathematical generality; they vanish in the physical cases, except $Q_{\tilde{T}}$ which does not vanish for the atmosphere and corresponds then to the solar heating.

We consider a uniformly stratified flow with constant velocity $\bar{\mathbf{v}}_0 = (\overline{U}_0,0)$, and the density, the pressure, and the temperature being of the form $\rho_0+\bar{\rho}_0(z)$, $p_0+\bar{p}_0(z)$ and $T_0+\overline{T}_0(z)$, with

$$\begin{cases} \bar{\rho}_0(z) = -\rho_0 N^2 g^{-1} z, \\ \overline{T}_0(z) = N^2(\alpha g)^{-1} z, \\ \bar{p}_{0z}(z) = -(\rho_0+\bar{\rho}_0)g. \end{cases} \tag{2.2}$$

Here N is the Brunt–Väisälä buoyancy frequency, assumed to be constant; ρ_0, p_0 and T_0 are respectively reference values of the density, pressure and temperature. We then decompose the unknowns of (2.1) in the form:

$$\begin{cases} \tilde{\mathbf{v}} = \bar{\mathbf{v}}_0 + \mathbf{v}(x,y,z,t), \\ \tilde{w} = w(x,y,z,t), \\ \tilde{\rho} = \rho_0 + \bar{\rho}_0 + \rho(x,y,z,t), \\ \tilde{T} = T_0 + \overline{T}_0 + T(x,y,z,t), \\ \tilde{p} = p_0 + \bar{p}_0 + p(x,y,z,t). \end{cases} \tag{2.3}$$

Substituting (2.3) into the system (2.1), and separating the linear and nonlinear terms, we obtain a system for u, v, w, ρ, T and p:

$$\begin{cases} u_t + \overline{U}_0 u_x - fv + \frac{1}{\rho_0}p_x + B(u,v,w;u) = 0, \\ v_t + \overline{U}_0 v_x + fu + \frac{1}{\rho_0}p_y + B(u,v,w;v) + f\overline{U}_0 = 0, \\ T_t + \overline{U}_0 T_x + \frac{N^2}{\alpha g}w + B(u,v,w;T) = 0, \\ p_z = -\rho g, \\ u_x + v_y + w_z = 0, \\ \rho = -\alpha\rho_0 T, \end{cases} \tag{2.4}$$

where for $\theta = u, v$ or T,

$$B(u,v,w;\theta) = u\theta_x + v\theta_y + w\theta_z. \tag{2.5}$$

We substitute $(2.4)_6$ into $(2.4)_4$, and set

$$\begin{cases} \phi = p/\rho_0, \\ \psi = \phi_z = \alpha T g. \end{cases} \tag{2.6}$$

After these steps we reach the following system with five equations and five unknowns:

$$\begin{cases} u_t + \overline{U}_0 u_x - fv + \phi_x + B(u,v,w;u) = 0, \\ v_t + \overline{U}_0 v_x + fu + \phi_y + B(u,v,w;v) + f\overline{U}_0 = 0, \\ \psi_t + \overline{U}_0\psi_x + N^2 w + B(u,v,w;\psi) = 0, \\ u_x + v_y + w_z = 0, \\ \phi_z = \psi, \end{cases} \tag{2.7}$$

where B is defined in (2.5).

2.1. The finite elements in the y-direction

We recall that in [3] three finite elements, that is, the hat functions h_1, h_2 and h_3 (see Fig. 2.1), were introduced in the y-direction. Instead of the usual hat function $\tilde{h}_2$ (see Fig. 2.1), h_2 was used so that h_1, h_2 and h_3 are *orthogonal*; this choice of h_2 (replacing $\tilde{h}_2$), which was inspired by work on wavelets [5], is essential.

We now look for approximate solutions of (2.7) of the form

$$\begin{cases} u = u_1(x,z,t)h_1(y) + u_2(x,z,t)h_2(y) + u_3(x,z,t)h_3(y), \\ v = v_1(x,z,t)h_1(y) + v_2(x,z,t)h_2(y) + v_3(x,z,t)h_3(y), \\ w = w_1(x,z,t)h_1(y) + w_2(x,z,t)h_2(y) + w_3(x,z,t)h_3(y), \\ \phi = \phi_1(x,z,t)h_1(y) + \phi_2(x,z,t)h_2(y) + \phi_3(x,z,t)h_3(y), \\ \psi = \psi_1(x,z,t)h_1(y) + \psi_2(x,z,t)h_2(y) + \psi_3(x,z,t)h_3(y) \end{cases} \tag{2.8}$$

and consider the corresponding finite element (Galerkin) approximation of (2.7). Before we present the approximate equations, we introduce the following notations, which shall enable us to write the approximate equations in a compact form; we set:

$$\begin{aligned} &\boldsymbol{u} = (u_1,u_2,u_3)^{\mathrm{T}}, \quad \boldsymbol{v} = (v_1,v_2,v_3)^{\mathrm{T}}, \quad \boldsymbol{\phi} = (\phi_1,\phi_2,\phi_3)^{\mathrm{T}}, \\ &\boldsymbol{\psi} = (\psi_1,\psi_2,\psi_3)^{\mathrm{T}}, \quad \boldsymbol{w} = (w_1,w_2,w_3)^{\mathrm{T}}. \end{aligned} \tag{2.9}$$

Then the Galerkin approximation to (2.7) reads

$$\begin{cases} \boldsymbol{u}_t + \overline{U}_0\boldsymbol{u}_x + \boldsymbol{\phi}_x - f\boldsymbol{v} + \mathbf{B}(\boldsymbol{u},\boldsymbol{v},\boldsymbol{w};\boldsymbol{u}) = 0, \\ \boldsymbol{v}_t + \overline{U}_0\boldsymbol{v}_x + f\boldsymbol{u} + \Lambda\boldsymbol{\phi} + \boldsymbol{f} + \mathbf{B}(\boldsymbol{u},\boldsymbol{v},\boldsymbol{w};\boldsymbol{v}) = 0, \\ \boldsymbol{\psi}_t + \overline{U}_0\boldsymbol{\psi}_x + N^2\boldsymbol{w} + \mathbf{B}(\boldsymbol{u},\boldsymbol{v},\boldsymbol{w};\boldsymbol{\psi}) = 0, \\ \boldsymbol{u}_x + \Lambda\boldsymbol{v} + \boldsymbol{w}_z = 0, \\ \boldsymbol{\psi} = \boldsymbol{\phi}_z, \end{cases} \tag{2.10}$$

where $\boldsymbol{\theta}$ taking the values of $\boldsymbol{u}$, $\boldsymbol{v}$ or $\boldsymbol{\psi}$,

$$\mathbf{B}(\boldsymbol{u},\boldsymbol{v},\boldsymbol{w};\boldsymbol{\theta}) = (B_1(\boldsymbol{u},\boldsymbol{v},\boldsymbol{w};\boldsymbol{\theta}), B_2(\boldsymbol{u},\boldsymbol{v},\boldsymbol{w};\boldsymbol{\theta}), B_3(\boldsymbol{u},\boldsymbol{v},\boldsymbol{w};\boldsymbol{\theta})) \tag{2.11}$$

and

$$\begin{cases} B_1(\boldsymbol{u},\boldsymbol{v},\boldsymbol{w};\boldsymbol{\theta}) = \boldsymbol{u}^{\mathrm{T}}\Gamma_1\boldsymbol{\theta}_x + \boldsymbol{v}^{\mathrm{T}}\Lambda_1\boldsymbol{\theta} + \boldsymbol{w}^{\mathrm{T}}\Gamma_1\boldsymbol{\theta}_z, \\ B_2(\boldsymbol{u},\boldsymbol{v},\boldsymbol{w};\boldsymbol{\theta}) = \boldsymbol{u}^{\mathrm{T}}\Gamma_2\boldsymbol{\theta}_x + \boldsymbol{v}^{\mathrm{T}}\Lambda_2\boldsymbol{\theta} + \boldsymbol{w}^{\mathrm{T}}\Gamma_2\boldsymbol{\theta}_z, \\ B_3(\boldsymbol{u},\boldsymbol{v},\boldsymbol{w};\boldsymbol{\theta}) = \boldsymbol{u}^{\mathrm{T}}\Gamma_3\boldsymbol{\theta}_x + \boldsymbol{v}^{\mathrm{T}}\Lambda_3\boldsymbol{\theta} + \boldsymbol{w}^{\mathrm{T}}\Gamma_3\boldsymbol{\theta}_z. \end{cases} \tag{2.12}$$

In (2.10) and (2.12) we used the following notations:

$$\Lambda = \frac{1}{L_2}\begin{pmatrix} -3 & -9 & 0 \\ \frac{1}{2} & 0 & -\frac{1}{2} \\ 0 & 9 & 3 \end{pmatrix}, \quad \boldsymbol{f} = \begin{pmatrix} \frac{3}{2}f\overline{U}_0 \\ -\frac{1}{2}f\overline{U}_0 \\ \frac{3}{2}f\overline{U}_0 \end{pmatrix},$$

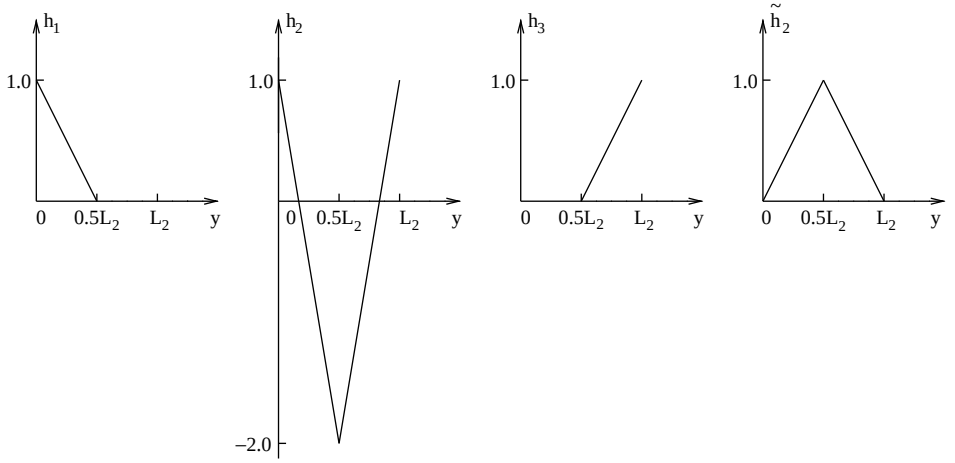

Fig. 2.1. The hat functions h_1, h_2, h_3 and $\tilde{h}_2$.

$$\Lambda_1 = \frac{1}{L_2}\begin{pmatrix} -2 & -6 & 0 \\ 0 & 0 & 0 \\ 0 & 0 & 0 \end{pmatrix}, \quad \Gamma_1 = \begin{pmatrix} \frac{3}{4} & \frac{1}{4} & 0 \\ \frac{1}{4} & \frac{3}{4} & 0 \\ 0 & 0 & 0 \end{pmatrix},$$
$$\Lambda_2 = \frac{1}{L_2}\begin{pmatrix} 0 & 0 & 0 \\ -1 & 0 & 1 \\ 0 & 0 & 0 \end{pmatrix}, \quad \Gamma_2 = \begin{pmatrix} \frac{1}{24} & \frac{1}{8} & 0 \\ \frac{1}{8} & -\frac{5}{4} & \frac{1}{8} \\ 0 & \frac{1}{8} & \frac{1}{24} \end{pmatrix},$$
$$\Lambda_3 = \frac{1}{L_2}\begin{pmatrix} 0 & 0 & 0 \\ 0 & 0 & 0 \\ 0 & 6 & 2 \end{pmatrix}, \quad \Gamma_3 = \begin{pmatrix} 0 & 0 & 0 \\ 0 & \frac{3}{4} & \frac{1}{4} \\ 0 & \frac{1}{4} & \frac{3}{4} \end{pmatrix}.$$

Note that the matrices Λ, Λ_1, Λ_2 and Λ_3 are the finite element representations of the differential operator $\partial/\partial y$ in the respective contexts, whereas Γ_1, Γ_2 and Γ_3 are matrix coefficients related to the nonlinear interactions.

2.2. The normal mode expansions

Following [14] and [21], we consider the normal mode expansion of the solutions of the system (2.10). That is, we look for the solutions written in the following form:

$$\begin{cases} (\boldsymbol{u}, \boldsymbol{v}, \boldsymbol{\phi}) = \sum_{n \geqslant 0} \mathcal{U}_n(z)(\boldsymbol{u}_n, \boldsymbol{v}_n, \boldsymbol{\phi}_n)(x,t), \\ (\boldsymbol{w}, \boldsymbol{\psi}) = \sum_{n \geqslant 1} \mathcal{W}_n(z)(\boldsymbol{w}_n, \boldsymbol{\psi}_n)(x,t). \end{cases} \tag{2.13}$$

Here $\boldsymbol{u}_n$, $\boldsymbol{v}_n$, etc., are vector functions like $\boldsymbol{u}$, $\boldsymbol{v}$, etc., but are *independent* of z. We refer the reader to [21] for the justification of the normal mode expansion. The specifications of the eigenfunctions $\mathcal{U}_n$ and $\mathcal{W}_n$ can be found in [3,18], and are repeated here for the readers' convenience:

$$\begin{cases} \mathcal{U}_0 = \sqrt{\frac{1}{H}}, \quad \text{and} \quad \mathcal{U}_n = \sqrt{\frac{2}{H}}\cos(\lambda_n N z) \quad \text{for } n \geqslant 1, \\ \mathcal{W}_n = \sqrt{\frac{2}{H}}\sin(\lambda_n N z) \quad \text{for } n \geqslant 1, \end{cases} \tag{2.14}$$

where $\lambda_n = n\pi/NH$. We observe that, for $n, m \geqslant 1$,

$$\begin{cases} \int_{-H}^{0} \mathcal{U}_n(z)\mathcal{U}_m(z)\mathrm{d}z = \delta_{n,m}, \\ \int_{-H}^{0} \mathcal{W}_n(z)\mathcal{W}_m(z)\mathrm{d}z = \delta_{n,m}, \\ \int_{-H}^{0} \mathcal{U}_n(z)\mathcal{W}_m(z)\mathrm{d}z = 0, \\ \mathcal{U}_n'(z) = -N\lambda_n \mathcal{W}_n(z), \\ \mathcal{W}_n'(z) = N\lambda_n \mathcal{U}_n(z). \end{cases} \tag{2.15}$$

Then we introduce the expansions (2.13) into the system (2.10). We classically derive from (2.10) an infinite system for the modes $\boldsymbol{u}_n$, $\boldsymbol{v}_n$, etc. Indeed, for each $n \geqslant 0$, we multiply each equation by $\mathcal{U}_n$ (or $\mathcal{W}_n$ for the 3rd and 5th equations), and integrate over $(-H, 0)$. For the zero mode ($n = 0$), we first carry out the following decomposition of $\boldsymbol{\phi}_0$ (see [3]); we write:

$$\boldsymbol{\phi}_0 = \bar{\boldsymbol{\phi}}_0 + \boldsymbol{\phi}_0', \tag{2.16}$$

where $\bar{\boldsymbol{\phi}}_0$, which is not unique, is one of the constant solutions of[2]

$$\Lambda \bar{\boldsymbol{\phi}}_0 = -\boldsymbol{f}_0 \tag{2.17}$$

with Λ defined in Section 2.1, and

$$\boldsymbol{f}_0 = \begin{pmatrix} \frac{3}{2} f \overline{U}_0 \sqrt{H} \\ -\frac{1}{2} f \overline{U}_0 \sqrt{H} \\ \frac{3}{2} f \overline{U}_0 \sqrt{H} \end{pmatrix}. \tag{2.18}$$

For simplicity, we write $\boldsymbol{\phi}_0$ instead of $\boldsymbol{\phi}_0'$ in the sequel. Thus the system for $\boldsymbol{u}_0$, $\boldsymbol{v}_0$ and $\boldsymbol{\phi}_0$ reads

$$\begin{cases} \boldsymbol{u}_{0t} + \overline{U}_0 \boldsymbol{u}_{0x} + \boldsymbol{\phi}_{0x} - f\boldsymbol{v}_0 + \mathbf{B}_0(\boldsymbol{u}, \boldsymbol{v}, \boldsymbol{w}; \boldsymbol{u}) = 0, \\ \boldsymbol{v}_{0t} + \overline{U}_0 \boldsymbol{v}_{0x} + f\boldsymbol{u}_0 + \Lambda\boldsymbol{\phi}_0 + \mathbf{B}_0(\boldsymbol{u}, \boldsymbol{v}, \boldsymbol{w}; \boldsymbol{v}) = 0, \\ \boldsymbol{u}_{0x} + \Lambda \boldsymbol{v}_0 = 0, \end{cases} \tag{2.19}$$

[2] That is, $\bar{\phi}_0$ is a discrete approximation of the geostrophic equation $\phi_y = -fu$, $u = \overline{U}_0$.

where for $\theta = \boldsymbol{u}$ or $\boldsymbol{v}$, and $n \geqslant 0$:

$$\mathbf{B}_n(\boldsymbol{u}, \boldsymbol{v}, \boldsymbol{w}; \theta) = \int_{-H}^{0} \mathbf{B}(\boldsymbol{u}, \boldsymbol{v}, \boldsymbol{w}; \theta) \mathcal{U}_n \, \mathrm{d}z. \tag{2.20}$$

For all modes $n \geqslant 1$, the systems that we obtain have the same form:

$$\begin{cases} \boldsymbol{u}_{nt} + \overline{U}_0 \boldsymbol{u}_{nx} + \boldsymbol{\phi}_{nx} - f\boldsymbol{v}_n + \mathbf{B}_n(\boldsymbol{u}, \boldsymbol{v}, \boldsymbol{w}; \boldsymbol{u}) = 0, \\ \boldsymbol{v}_{nt} + \overline{U}_0 \boldsymbol{v}_{nx} + f\boldsymbol{u}_n + \Lambda \boldsymbol{\phi}_n + \mathbf{B}_n(\boldsymbol{u}, \boldsymbol{v}, \boldsymbol{w}; \boldsymbol{v}) = 0, \\ \boldsymbol{\psi}_{nt} + \overline{U}_0 \boldsymbol{\psi}_{nx} + N^2 \boldsymbol{w}_n + \mathbf{B}_n^{\#}(\boldsymbol{u}, \boldsymbol{v}, \boldsymbol{w}; \boldsymbol{\psi}) = 0, \\ \boldsymbol{u}_{nx} + \Lambda \boldsymbol{v}_n + N\lambda_n \boldsymbol{w}_n = 0, \\ -N\lambda_n \boldsymbol{\phi}_n = \boldsymbol{\psi}_n, \end{cases} \tag{2.21}$$

where for $\theta = \boldsymbol{u}, \boldsymbol{v}$, and $n \geqslant 1$, $\mathbf{B}_n(\boldsymbol{u}, \boldsymbol{v}, \boldsymbol{w}; \theta)$ were already defined in (2.20), and

$$\mathbf{B}_n^{\#}(\boldsymbol{u}, \boldsymbol{v}, \boldsymbol{w}; \boldsymbol{\psi}) = \int_{-H}^{0} \mathbf{B}(\boldsymbol{u}, \boldsymbol{v}, \boldsymbol{w}; \boldsymbol{\psi}) \mathcal{W}_n \, \mathrm{d}z, \quad n \geqslant 1. \tag{2.22}$$

From the last two equations in (2.21) we infer that

$$\boldsymbol{\phi}_n = -\frac{1}{N\lambda_n} \boldsymbol{\psi}_n, \quad \boldsymbol{w}_n = -\frac{1}{N\lambda_n} (\boldsymbol{u}_{nx} + \Lambda \boldsymbol{v}_n), \tag{2.23}$$

which means that $\boldsymbol{\phi}_n$ and $\boldsymbol{w}_n$ are diagnostic variables fully determined by the other three unknowns. We can thus eliminate $\boldsymbol{\phi}_n$ and $\boldsymbol{w}_n$ from (2.21), and obtain a system for $\boldsymbol{u}_n$, $\boldsymbol{v}_n$ and $\boldsymbol{\psi}_n$, for each $n \geqslant 1$:

$$\begin{cases} \boldsymbol{u}_{nt} + \overline{U}_0 \boldsymbol{u}_{nx} - \frac{1}{N\lambda_n} \boldsymbol{\psi}_{nx} - f\boldsymbol{v}_n + \mathbf{B}_n(\boldsymbol{u}, \boldsymbol{v}, \boldsymbol{w}; \boldsymbol{u}) = 0, \\ \boldsymbol{v}_{nt} + \overline{U}_0 \boldsymbol{v}_{nx} + f\boldsymbol{u}_n - \frac{1}{N\lambda_n} \Lambda \boldsymbol{\psi}_n + \mathbf{B}_n(\boldsymbol{u}, \boldsymbol{v}, \boldsymbol{w}; \boldsymbol{v}) = 0, \\ \boldsymbol{\psi}_{nt} - \frac{N}{\lambda_n} \boldsymbol{u}_{nx} + \overline{U}_0 \boldsymbol{\psi}_{nx} - \frac{N}{\lambda_n} \Lambda \boldsymbol{v}_n + \mathbf{B}_n(\boldsymbol{u}, \boldsymbol{v}, \boldsymbol{w}; \boldsymbol{\psi}) = 0. \end{cases} \tag{2.24}$$

2.3. Boundary conditions and the well-posedness for the linearized initial-boundary value problem

For the linearized model in [3] we assume that the perturbation variables u, v etc., as well as their first order derivatives, are small compared to their reference values (e.g. u is small compared to $\overline{U}_0$). This assumption leads us to the linearized version of the system (2.7):

$$\begin{cases} u_t + \overline{U}_0 u_x - fv + \phi_x = 0, \\ v_t + \overline{U}_0 v_x + fu + \phi_y + f\overline{U}_0 = 0, \\ \psi_t + \overline{U}_0 \psi_x + N^2 w = 0, \\ u_x + v_y + w_z = 0, \\ \phi_z = \psi. \end{cases} \tag{2.25}$$

We then perform on this linearized system the finite element expansion and normal mode decomposition, as described in the previous two subsections. We thus obtain the linearized versions of (2.19) and (2.24), that is, for $n = 0$,

$$\begin{cases} \boldsymbol{u}_{0t} + \overline{U}_0 \boldsymbol{u}_{0x} + \boldsymbol{\phi}_{0x} - f\boldsymbol{v}_0 = 0, \\ \boldsymbol{v}_{0t} + \overline{U}_0 \boldsymbol{v}_{0x} + f\boldsymbol{u}_0 + \Lambda \boldsymbol{\phi}_0 = 0, \\ \boldsymbol{u}_{0x} + \Lambda \boldsymbol{v}_0 = 0 \end{cases} \tag{2.26}$$

and for $n \geqslant 1$,

$$\begin{cases} \boldsymbol{u}_{nt} + \overline{U}_0 \boldsymbol{u}_{nx} - \frac{1}{N\lambda_n} \boldsymbol{\psi}_{nx} - f\boldsymbol{v}_n = 0, \\ \boldsymbol{v}_{nt} + \overline{U}_0 \boldsymbol{v}_{nx} + f\boldsymbol{u}_n - \frac{1}{N\lambda_n} \Lambda \boldsymbol{\psi}_n = 0, \\ \boldsymbol{\psi}_{nt} - \frac{N}{\lambda_n} \boldsymbol{u}_{nx} + \overline{U}_0 \boldsymbol{\psi}_{nx} - \frac{N}{\lambda_n} \Lambda \boldsymbol{v}_n = 0. \end{cases} \tag{2.27}$$

In [3], a set of modal boundary conditions were proposed for the systems (2.26) and (2.27), and the well-posedness of the corresponding linearized initial value problem was shown. We shall recall those boundary conditions for (2.27) in this subsection; but the treatment, as well as the boundary conditions, of the zero mode (2.26) will be different than in [3] so that it is more suitable for the numerical simulations.

The coefficient matrix of the first order derivatives in (2.27) has three eigenvalues $\overline{U}_0 + 1/\lambda_n$, $\overline{U}_0$ and $\overline{U}_0 - 1/\lambda_n$. The first two are always positive, while depending on n the third eigenvalue $\overline{U}_0 - 1/\lambda_n$ can be either positive or negative for the actual (physical) values of the parameters $\overline{U}_0$, L_1, H, etc. We say that the corresponding mode is supercritical if $\overline{U}_0 - \lambda_n^{-1} > 0$, and subcritical otherwise. The supercritical modes require three boundary conditions at $x = 0$, and the subcritical modes require

two boundary conditions at $x = 0$ and one at $x = L_1$. This mandates that we impose different boundary conditions according to the type of the modes.

We first note that the sequence $\{\lambda_n\}$ is monotone and $\lambda_n \to \infty$ as $n \to \infty$. Therefore, there are only a finite number of subcritical modes, and we denote this finite number by n_c. For physically relevant values of the data, n_c is ranging, say, from 1 to 10.

Let ξ_n, $\boldsymbol{v}_n$ and η_n be the eigenvectors corresponding to $\overline{U}_0 + 1/\lambda_n$, $\overline{U}_0$ and $\overline{U}_0 - 1/\lambda_n$, respectively. Specifically we choose

$$\begin{cases} \xi_n = \boldsymbol{u}_n - \psi_n/N, \\ \boldsymbol{v}_n = \boldsymbol{v}_n, \\ \eta_n = \boldsymbol{u}_n + \psi_n/N. \end{cases} \tag{2.28}$$

With this new set of unknowns we transform the system (2.27) into the following form:

$$\begin{cases} \xi_{nt} + (\overline{U}_0 + \frac{1}{\lambda_n})\xi_{nx} + \left(-f + \frac{\Lambda}{\lambda_n}\right)\boldsymbol{v}_n = 0, \\ \boldsymbol{v}_{nt} + \overline{U}_0 \boldsymbol{v}_{nx} + \left(\frac{f}{2} + \frac{\Lambda}{2\lambda_n}\right)\xi_n + \left(\frac{f}{2} - \frac{\Lambda}{2\lambda_n}\right)\eta_n = 0, \\ \eta_{nt} + \left(\overline{U}_0 - \frac{1}{\lambda_n}\right)\eta_{nx} + \left(-f - \frac{\Lambda}{\lambda_n}\right)\boldsymbol{v}_n = 0. \end{cases} \tag{2.29}$$

Neglecting the lower order terms we see that the equations in (2.29) are all of the form $r_t + \alpha r_x = 0$. We know that the natural boundary condition for such an equation is to prescribe r at $x = 0$ if $\alpha > 0$ and to prescribe r at $x = L_1$ if $\alpha < 0$ (the parts of the boundary where the characteristics enter the domain). We observe that $\alpha > 0$ for all the equations (2.29), except for η_n when $\overline{U}_0 - \lambda_n^{-1} < 0$, that is for the subcritical modes. Thus following [3] the boundary conditions are imposed in the following way. For the supercritical modes, i.e. when $n > n_c$, we take the natural boundary conditions,

$$\begin{cases} \xi_n(0,t) = 0, \\ \boldsymbol{v}_n(0,t) = 0, \\ \eta_n(0,t) = 0 \end{cases} \tag{2.30}$$

and for the subcritical modes, i.e. when $1 \leqslant n \leqslant n_c$,

$$\begin{cases} \xi_n(0,t) = 0, \\ \boldsymbol{v}_n(0,t) = 0, \\ \eta_n(L_1,t) = 0. \end{cases} \tag{2.31}$$

The well-posedness of the initial-boundary value problem associated with the linear system (2.25), with the zero mode excluded, was established in [3] using the linear semigroup theory (Hille–Yosida theorem).

For the zero mode (see (2.26)) we depart from [3] and choose the following boundary conditions:

$$\begin{cases} \boldsymbol{u}_0(0,t) = \boldsymbol{u}_0^l(t), \\ \boldsymbol{v}_0(0,t) = \boldsymbol{v}_0^l(t), \\ \phi_0(0,t) = \phi_0^l(t), \\ \phi_0(L_1,t) = \phi_0^r(t), \end{cases} \tag{2.32}$$

where $\boldsymbol{u}_0^l(t)$, $\boldsymbol{v}_0^l(t)$, $\phi_0^l(t)$ and $\phi_0^r(t)$ are given[3] functions of t. The choice of this set of boundary conditions will be justified below.

Let[4]

$$\zeta_0(x,t) = \Lambda \boldsymbol{u}_0 - \boldsymbol{v}_{0,x}. \tag{2.33}$$

Then apply the operator Λ to $(2.26)_1$ and the operator $\partial/\partial x$ to $(2.26)_2$, and subtract the resulting equations. This gives

$$\frac{\partial}{\partial t}\zeta_0 + \overline{U}_0 \frac{\partial}{\partial x}\zeta_0 = 0. \tag{2.34}$$

The value of ζ_0 at $t = 0$ can be computed from the given initial condition; and the value of ζ_0 at $x = 0$ can be computed from the given boundary conditions (see [3], Section 3.4, for more details). Hence Eq. (2.34) can be solved. Once we have ζ_0, we can solve the following ODE system for $\boldsymbol{u}_0$ and $\boldsymbol{v}_0$:

$$\begin{cases} \boldsymbol{u}_{0x} + \Lambda \boldsymbol{v}_0 = 0, \\ \boldsymbol{v}_{0x} - \Lambda \boldsymbol{u}_0 = -\zeta_0. \end{cases} \tag{2.35}$$

[3] At this stage $\phi_0^r(t)$ is left free; see Section 2.5 for the geostrophic boundary condition.

[4] Since Λ is the discrete form of $\partial/\partial y$, $\Lambda \boldsymbol{u}_0 - \boldsymbol{v}_{0,x}$ is the discrete form of $\mathrm{curl}(\boldsymbol{u}_0, \boldsymbol{v}_0)$.

For ϕ_0, as we said, we take an approach different from that in [3]. We use the first two equations of (2.26) (instead of the first one only). We differentiate the first equation in x, apply the operator Λ to the second one, and add the resulting equations to find:

$$\phi_{0xx} + \Lambda^2 \phi_0 = -f\zeta_0. \tag{2.36}$$

It is shown in Appendix A that the equation above, supplemented with the boundary conditions $(2.32)_{3,4}$, has a unique solution for every ζ_0 sufficiently regular. Note that (2.36) is a differential equation in x, and t is a parameter in (2.36).

2.4. Modal boundary conditions for the nonlinear problem

In this subsection we consider the full nonlinear Eq. (2.7) and their modal expansions (2.19) and (2.21), and we show how to implement the same boundary conditions as in the linear case.

We perform the same change of variables (2.28) and we deduce from (2.21) the equations:

$$\begin{cases} \xi_{nt} + (\overline{U}_0 + \frac{1}{\lambda_n})\xi_{nx} + \left(-f + \frac{\Lambda}{\lambda_n}\right)\boldsymbol{v}_n + \mathrm{NL}_{\xi_n} = 0, \\ \boldsymbol{v}_{nt} + \overline{U}_0 \boldsymbol{v}_{nx} + \left(\frac{f}{2} + \frac{\Lambda}{2\lambda_n}\right)\xi_n + \left(\frac{f}{2} - \frac{\Lambda}{2\lambda_n}\right)\eta_n + \mathrm{NL}_{\boldsymbol{v}_n} = 0, \\ \eta_{nt} + (\overline{U}_0 - \frac{1}{\lambda_n})\eta_{nx} + (-f - \frac{\Lambda}{\lambda_n})\boldsymbol{v}_n + \mathrm{NL}_{\eta_n} = 0, \end{cases} \tag{2.37}$$

where

$$\begin{cases} \mathrm{NL}_{\xi_n} = \mathbf{B}_n(\boldsymbol{u}, \boldsymbol{v}, \boldsymbol{w}; \boldsymbol{u}) - \frac{1}{N}\mathbf{B}_n(\boldsymbol{u}, \boldsymbol{v}, \boldsymbol{w}; \psi), \\ \mathrm{NL}_{\boldsymbol{v}_n} = \mathbf{B}_n(\boldsymbol{u}, \boldsymbol{v}, \boldsymbol{w}; \boldsymbol{v}), \\ \mathrm{NL}_{\eta_n} = \mathbf{B}_n(\boldsymbol{u}, \boldsymbol{v}, \boldsymbol{w}; \boldsymbol{u}) + \frac{1}{N}\mathbf{B}_n(\boldsymbol{u}, \boldsymbol{v}, \boldsymbol{w}; \psi). \end{cases} \tag{2.38}$$

The nonlinear equations of the zero mode are still (2.19). Our treatment of this system is analogous to that of the linear system (2.26). Indeed, with ζ_0 defined as in (2.33), we first obtain the equation for ζ_0 from the first two equations of (2.19):

$$\frac{\partial}{\partial t}\zeta_0 + \overline{U}_0 \frac{\partial}{\partial x}\zeta_0 + \Lambda \mathbf{B}_0(\boldsymbol{u}, \boldsymbol{v}, \boldsymbol{w}; \boldsymbol{u}) - \frac{\partial}{\partial x}\mathbf{B}_0(\boldsymbol{u}, \boldsymbol{v}, \boldsymbol{w}; \boldsymbol{v}) = 0. \tag{2.39}$$

In the nonlinear case, all modes are coupled and the zero mode cannot be treated independently of the modes $n \geqslant 1$ since e.g. in (2.39), the terms B_0 contains the modes $n \geqslant 0$. The following remarks are related to the numerical treatment of (2.37)–(2.39), and not related to the theoretical issues such as existence of and uniqueness of solutions. Hence for the numerical approximation of (2.39) at time t_{n+1}, if we treat the nonlinear terms explicitly (that is, using e.g. their values at time t_n), we can advance Eq. (2.39) in ζ_0 by supplementing it with boundary and initial conditions as in the linear case. Once ζ_0 is known at time t_{n+1}, we can determine $\boldsymbol{u}_0$ and $\boldsymbol{v}_0$ at time t_{n+1} by solving the following ODE system:

$$\begin{cases} \boldsymbol{u}_{0x} + \Lambda \boldsymbol{v}_0 = 0, \\ \boldsymbol{v}_{0x} - \Lambda \boldsymbol{u}_0 = -\zeta_0. \end{cases} \tag{2.40}$$

Finally, we combine the first two equations of (2.19) again to obtain an equation for ϕ_0:

$$\phi_{0xx} + \Lambda^2 \phi_0 = -f\zeta_0 - \frac{\partial}{\partial x}\mathbf{B}(\boldsymbol{u}, \boldsymbol{v}, \boldsymbol{w}; \boldsymbol{u}) - \Lambda \mathbf{B}(\boldsymbol{u}, \boldsymbol{v}, \boldsymbol{w}; \boldsymbol{v}). \tag{2.41}$$

We supplement Eq. (2.41) with boundary conditions similar to $(2.32)_3$ and $(2.32)_4$ (see below in Section 2.5), and we treat the nonlinear terms explicitly (using known values); we then infer ϕ_0 at time t_{n+1}, and now all values $\boldsymbol{u}_0$, $\boldsymbol{v}_0$, ϕ_0 have been advanced.

In what precedes and in the following we assume that the initial data are such that the nonlinear parts are small compared to the linear parts, so that the characteristic values do not change sign, at least for a certain period of time. Assuming so, we conjecture that the boundary conditions which lead to the well-posedness of the linearized system will also furnish a well-posed problem for the nonlinear equations, at least for some time. We leave the theoretical analysis to subsequent studies, and perform here the corresponding numerical simulations based on this hypothesis, which is comforted by the lack of numerical blow-up. Hence the boundary conditions that we consider for the nonlinear problems are (2.30)–(2.32).

2.5. Geostrophic boundary conditions for ϕ_0

We recall that ϕ_0 is actually ϕ_0', which is a small perturbation to the geostrophic solution $\bar{\phi}_0$ of (2.17). To make our model physically more interesting, we want ϕ_0' to be close to being geostrophic too. Remember that the boundary value function ϕ_0^r in $(2.32)_4$ has been left free so far. Hence we have the freedom to impose certain restrictions on it. We choose to compute ϕ_0^r from the known quantities $\boldsymbol{u}_0$ and $\boldsymbol{v}_0$[5] by the geostrophic equations (see below), in the hope that, with this specially prepared

[5] These quantities and known at time t_{n+1} when we compute ϕ_0' at time t_{n+1}; see the explanation above.

boundary condition, the solution ϕ_0 will stay close to being geostrophic. We shall denote this new boundary value function as $\phi^r_{0,g}$ (g for geostrophic) to distinguish it from the previous notation ϕ^r_0.

In order to calculate $\phi^r_{0,g}$ we need to introduce the scalar functions $u_0(x,y,t)$, $v_0(x,y,t)$ and $\phi_0(x,y,t)$. They are related to $\boldsymbol{u}_0$, $\boldsymbol{v}_0$ and $\boldsymbol{\phi}_0$ (see (2.8) and (2.13)) by the following equations:

$$\begin{cases} u_0(x,y,t) = u_{01}(x,t)h_1(y) + u_{02}(x,t)h_2(y) + u_{03}(x,t)h_3(y), \\ v_0(x,y,t) = v_{01}(x,t)h_1(y) + v_{02}(x,t)h_2(y) + v_{03}(x,t)h_3(y), \\ \phi_0(x,y,t) = \phi_{01}(x,t)h_1(y) + \phi_{02}(x,t)h_2(y) + \phi_{03}(x,t)h_3(y), \end{cases} \tag{2.42}$$

where h_1, etc., are the hat functions introduced in Section 2.1 (see Fig. 2.1). We observe that if $u_{0,1}$, etc. are known, we can compute u_0, etc. from (2.42), and on the other hand, if u_0, etc. are known, and if they are linear in y, then we can compute u_{01}, etc. from (2.42) too. The geostrophic equations for u_0, v_0 and ϕ_0 read

$$\begin{cases} -fv_0 + \phi_{0x} = 0, \\ fu_0 + \phi_{0y} = 0. \end{cases} \tag{2.43}$$

After these reminders, we are ready to sketch the procedure for calculating $\phi^r_{0,g}$. For each time $t \in (0,T)$ (e.g. $t = t_{n+1}$), we first find u_0 and v_0 from $\boldsymbol{u}_0$ and $\boldsymbol{v}_0$ by $(2.42)_{1,2}$, once the latter are known. Then we set $y = 0$, and integrate $(2.43)_1$ in x to find $\phi_0(L_1,0,t)$.[6] With $\phi_0(L_1,0,t)$ at hand, we can integrate $(2.43)_2$ in y to find $\phi_0(L_1,y,t)$ for every $y \in [0,L_2]$. Then we use $(2.42)_3$ to determine $\phi_{01}(L_1,t)$, $\phi_{02}(L_1,t)$ and $\phi_{03}(L_1,t)$, for every $t \in (0,T)$. These values are the three components of $\phi^r_{0,g}(t)$. The calculations are straightforward and easy, and so the details are skipped.

In the sequel we replace ϕ^r_0 on the right-hand side of $(2.32)_4$ by $\phi^r_{0,g}$, that is, the boundary values of ϕ_0 on the right boundary are to be calculated from the known quantities and the geostrophic Eq. (2.43).

3. Numerical scheme

3.1. Vertical discretization by spectral method

In the vertical direction, we proceed by normal modes decomposition as in (2.13). From the numerical point of view, we will need to transform some grid data into modal coefficients in the $\mathcal{U}_n$ or $\mathcal{W}_n$ bases of $\mathbf{L}^2(-H,0)$, and *vice versa*.

Given a function f represented by its values on a grid $z_l = -H + l\Delta z$, $0 \leqslant l \leqslant l_{\max}$, $\Delta z = H/l_{\max}$, we want to transform it into coefficients f_n, $0 \leqslant m \leqslant M$. To this aim we use the trapezoidal integration method, with the z_l as nodal points. For the functions $\boldsymbol{u}$, $\boldsymbol{v}$ and $\boldsymbol{\phi}$, we decompose them in the $\mathcal{U}_n$ basis of $\mathbf{L}^2(-H,0)$. For $0 \leqslant n \leqslant N_{\max}$:

$$\begin{aligned} \{\boldsymbol{u}_n, \boldsymbol{v}_n, \boldsymbol{\phi}_n\} &= \int_{-H}^{0} \mathcal{U}_n(z)\{\boldsymbol{u},\boldsymbol{v},\boldsymbol{\phi}\}(x,z,t)\mathrm{d}z \\ &= (\text{by trapezoidal rule}) \\ &\cong \frac{\Delta z}{2}\left(\mathcal{U}_n(z_0)\{\boldsymbol{u},\boldsymbol{v},\boldsymbol{\phi}\}(z_0) + \mathcal{U}_n(z_{\max})\{\boldsymbol{u},\boldsymbol{v},\boldsymbol{\phi}\}(z_{l_{\max}})\right) + \Delta z \sum_{l=1}^{l_{\max}-1} \mathcal{U}_n(z_l)\{\boldsymbol{u},\boldsymbol{v},\boldsymbol{\phi}\}(z_l) \end{aligned} \tag{3.1}$$

and for $\boldsymbol{w}$ and ψ, $1 \leqslant n \leqslant N_{\max}$:

$$\begin{aligned} \{\boldsymbol{w}_n, \psi_n\} &= \int_{-H}^{0} \mathcal{W}_n(z)\{\boldsymbol{w},\psi\}(x,z,t)\mathrm{d}z \\ &= (\text{by trapezoidal rule}) \\ &\cong \frac{\Delta z}{2}\left(\mathcal{W}_n(z_0)\{\boldsymbol{w},\psi\}(z_0) + \mathcal{W}_n(z_{\max})\{\boldsymbol{w},\psi\}(z_{l_{\max}})\right) + \Delta z \sum_{l=1}^{l_{\max}-1} \mathcal{W}_n(z_l)\{\boldsymbol{w},\psi\}(z_l) \end{aligned} \tag{3.2}$$

Alternatively, if the function is given by its modal coefficients, the values on the z-grid z_l, $0 \leqslant l \leqslant l_{\max}$ are simply given by:

$$\begin{cases} (\boldsymbol{u},\boldsymbol{v},\boldsymbol{\phi})(z_l) = \sum_{n \geqslant 0} \mathcal{U}_n(z_l)(\boldsymbol{u}_n,\boldsymbol{v}_n,\boldsymbol{\phi}_n), \\ (\boldsymbol{w},\psi)(z_l) = \sum_{n \geqslant 1} \mathcal{W}_n(z)(\boldsymbol{w}_n,\psi_n). \end{cases} \tag{3.3}$$

In the numerical simulations, we are given some initial data on the physical grid z_l, $0 \leqslant l \leqslant l_{\max}$. We transform them into modal coefficients thanks to formulas (3.1), and, in the linear case, we keep them all along the computations, except for graphic purposes, for which, we use the inverse formulas (3.2) to return to the physical space. Generally speaking, for the nonlinear problem, we need to operate (3.1) and (3.2) once at every time step, in order to avoid the computation of the convolution products, which would cost too much in terms of CPU time and is not considered an appropriate numerical

[6] Remember that $\phi_0(0,0,t)$ is known (prescribed).

procedure. But in our case, since we only take a small number of modes (at most 10), it is more convenient to compute the nonlinear terms by the convolution formulas. The latter approach is what we will take.

3.2. Finite difference method in time and space (x-direction only)

We choose to discretize the system (2.37) by finite differences in time and in the horizontal direction. Naturally care has to be taken of the sign of the characteristic values, in order to take an upwind (hence stable in the linear case) spatial discretization of the x-derivative. Whereas $\overline{U}_0$ and $\overline{U}_0 + 1/\lambda_n$ are always positive, the third characteristic value of the nth mode in the linear case is $\overline{U}_0 - 1/\lambda_n$, and it can either be positive or negative for the actual physical values that we consider.

In the nonlinear case, since the initial data are taken small compared to $\overline{U}_0$, we implicitly assume that the signs of the characteristic values remain unchanged for a certain period of time. Hence we conjecture that a stable scheme for the linear equations will remain stable for the nonlinear equations for a certain period of time.

The scheme that we choose for (2.37) is semi-implicit in time, that is, the first order x-derivatives are treated implicitly (in time), while the zero order terms and the nonlinear terms (for the nonlinear equations only) are treated explicitly (in time). The scheme is then as follows:

For every subcritical mode $1 \leqslant n \leqslant n_c$:

$$\begin{cases} \frac{\xi_{n,m}^{k+1}-\xi_{n,m}^{k}}{\Delta t} + \left(\overline{U}_0 + \frac{1}{\lambda_n}\right)\frac{\xi_{n,m}^{k+1}-\xi_{n,m-1}^{k+1}}{\Delta x} + \left(\frac{\Lambda}{\lambda_n} - f\right)\boldsymbol{v}_{n,m}^{k} + \mathrm{NL}_{\xi_{n,m}}^{k} = 0, \\ \frac{\boldsymbol{v}_{n,m}^{k+1}-\boldsymbol{v}_{n,m}^{k}}{\Delta t} + \overline{U}_0\frac{\boldsymbol{v}_{n,m}^{k+1}-\boldsymbol{v}_{n,m-1}^{k+1}}{\Delta x} + \left(\frac{f}{2} + \frac{\Lambda}{2\lambda_n}\right)\boldsymbol{\xi}_{n,m}^{k} + \left(\frac{f}{2} - \frac{\Lambda}{2\lambda_n}\right)\boldsymbol{\eta}_{n,m}^{k} + \mathrm{NL}_{\boldsymbol{v}_{n,m}}^{k} = 0, \\ \frac{\eta_{n,m}^{k+1}-\eta_{n,m}^{k}}{\Delta t} + \left(\overline{U}_0 - \frac{1}{\lambda_n}\right)\frac{\eta_{n,m+1}^{k+1}-\eta_{n,m}^{k+1}}{\Delta x} + \left(-f - \frac{\Lambda}{\lambda_n}\right)\boldsymbol{v}_{n,m}^{k} + \mathrm{NL}_{\eta_{n,m}}^{k} = 0, \end{cases} \tag{3.4}$$

where $1 \leqslant m \leqslant M$ for the first two equations, and $0 \leqslant m \leqslant M-1$ for the last equation.

For the supercritical modes $n > n_c$:

$$\begin{cases} \frac{\xi_{n,m}^{k+1}-\xi_{n,m}^{k}}{\Delta t} + \left(\overline{U}_0 + \frac{1}{\lambda_n}\right)\frac{\xi_{n,m}^{k+1}-\xi_{n,m-1}^{k+1}}{\Delta x} + \left(\frac{\Lambda}{\lambda_n} - f\right)\boldsymbol{v}_{n,m}^{k} + \mathrm{NL}_{\xi_{n,m}}^{k} = 0, \\ \frac{\boldsymbol{v}_{n,m}^{k+1}-\boldsymbol{v}_{n,m}^{k}}{\Delta t} + \overline{U}_0\frac{\boldsymbol{v}_{n,m}^{k+1}-\boldsymbol{v}_{n,m-1}^{k+1}}{\Delta x} + \left(\frac{f}{2} + \frac{\Lambda}{2\lambda_n}\right)\boldsymbol{\xi}_{n,m}^{k} + \left(\frac{f}{2} - \frac{\Lambda}{2\lambda_n}\right)\boldsymbol{\eta}_{n,m}^{k} + \mathrm{NL}_{\boldsymbol{v}_{n,m}}^{k} = 0, \\ \frac{\eta_{n,m}^{k+1}-\eta_{n,m}^{k}}{\Delta t} + \left(\overline{U}_0 - \frac{1}{\lambda_n}\right)\frac{\eta_{n,m}^{k+1}-\eta_{n,m-1}^{k+1}}{\Delta x} + \left(-f - \frac{\Lambda}{\lambda_n}\right)\boldsymbol{v}_{n,m}^{k} + \mathrm{NL}_{\eta_{n,m}}^{k} = 0, \end{cases} \tag{3.5}$$

where $1 \leqslant m \leqslant M$ for all three equations. In fact the only difference between Eqs. (3.4) and (3.5) appears in the upwind differentiation in x of $\boldsymbol{\eta}_x$.

The system for the zero mode is resolved in several steps. First we discretize (2.39) using a semi-implicit, first order scheme. The scheme reads, for $2 \leqslant m \leqslant M+1$,

$$\frac{\zeta_{0,m}^{k+1}-\zeta_{0,m}^{k}}{\Delta t} + \overline{U}_0\frac{\zeta_{0,m}^{k+1}-\zeta_{0,m-1}^{k+1}}{\Delta x} + \Lambda\mathbf{B}_{0,m}^{k}(\boldsymbol{u},\boldsymbol{v},\boldsymbol{w};\boldsymbol{u}) - \frac{\mathbf{B}_{0,m}^{k}(\boldsymbol{u},\boldsymbol{v},\boldsymbol{w};\boldsymbol{v}) - \mathbf{B}_{0,m-1}^{k}(\boldsymbol{u},\boldsymbol{v},\boldsymbol{w};\boldsymbol{v})}{\Delta x} = 0. \tag{3.6}$$

Once we have the discrete values of ζ_0, we discretize (2.40) for $\boldsymbol{u}_0$ and $\boldsymbol{v}_0$, using an explicit (in x), first-order scheme:

$$\begin{cases} \frac{\boldsymbol{u}_{0,m}^{k+1}-\boldsymbol{u}_{0,m-1}^{k+1}}{\Delta x} + \Lambda\boldsymbol{v}_{0,m-1}^{k+1} = 0, \\ \frac{\boldsymbol{v}_{0,m}^{k+1}-\boldsymbol{v}_{0,m-1}^{k+1}}{\Delta x} - \Lambda\boldsymbol{u}_{0,m-1}^{k+1} = -\boldsymbol{\zeta}_{0,m}^{k+1}, \end{cases} \tag{3.7}$$

where $\zeta_{0,m}^{k+1}$ is the value of the function ζ at grid point $((m-1)\Delta x, (k+1)\Delta t)$. Finally, we discretize (2.41) using the centered difference scheme. For $1 \leqslant m \leqslant M-1$,

$$\frac{\boldsymbol{\phi}_{0,m+1}^{k+1} - 2\boldsymbol{\phi}_{0,m}^{k+1} + \boldsymbol{\phi}_{0,m-1}^{k+1}}{\Delta x^2} + \Lambda^2\boldsymbol{\phi}_{0,m}^{k+1} = -f\boldsymbol{\zeta}_{0,m}^{k+1} - \frac{\mathbf{B}_{0,m}^{k+1}(\boldsymbol{u},\boldsymbol{v},\boldsymbol{w};\boldsymbol{u}) - \mathbf{B}_{0,m-1}^{k+1}(\boldsymbol{u},\boldsymbol{v},\boldsymbol{w};\boldsymbol{u})}{\Delta x} - \Lambda\mathbf{B}_{0,m}^{k+1}(\boldsymbol{u},\boldsymbol{v},\boldsymbol{w};\boldsymbol{v}). \tag{3.8}$$

Note that $\boldsymbol{\phi}_{0,0}^{k+1}$ and $\boldsymbol{\phi}_{0,M}^{k+1}$ are given by the boundary conditions $(2.32)_{3,4}$, and therefore the number of unknowns equals the number of equations in (3.8). The system can be easily inverted by a linear solver for band square matrices.

4. Numerical simulations

Two different simulations are performed. The first one is carried out on the larger domain $\Omega_0 = (0, L_1) \times (-H, 0)$ (see Fig. 4.1), and a set of *homogeneous* boundary conditions are prescribed at $x = 0, L_1$. This simulation is described and the results are presented in details in Section 4.1. The data obtained through this simulation will provide the *nonhomogeneous* boundary conditions for the second simulation on the middle half domain, designated as Ω_1 (see also (4.1)), of Ω_0. This simulation is described, and the results are presented in details in Section 4.2. Of course the first simulation itself supports the conjecture that the prescribed boundary conditions (2.30) and (2.31) are appropriate for the nonlinear problem at hand. The

purpose of the second simulation is to investigate the validity of the proposed boundary conditions for numerical simulations in a limited area with a nonphysical boundary. Here of course we ought to consider nonhomogeneous boundary conditions at the boundary, namely those given by the parent problem (simulation in Ω_0). In Section 4.3 the results from the two simulations are compared, and the coincidence of the results demonstrates the transparent properties of the boundary conditions prescribed.

The physical parameters that we used in the simulations are the following ones: $L_1 = 1000$ km, $L_2 = 500$ km, $H = 10$ km. We take the constant reference velocity $\overline{U}_0 = 20$ m/s, the Coriolis parameter $f = 10^{-4}$, and the Brunt–Väisälä buoyancy frequency $N = 10^{-2}$, which are typical of the mid-latitudes. We take 10,000 segments along $[0, L_1]$ in the x-direction. The final time for the simulation is $T = 50,000$ s, and we take 10,000 time steps. In the vertical direction we take 53 segments. In the computations we will deal with $N_{\max} = 5$ (the number of modes), which is sufficient from the physical point of view.

4.1. Simulation on the larger domain

We first recall that the scalar functions u, v, etc., are related to the vector functions $\boldsymbol{u}$, $\boldsymbol{v}$, etc. (see (2.9)), via Eq. (2.8). In the simulation the initial conditions are given for these scalar functions:

$$\begin{cases} u(x,y,z,0) = \sin^3\left(\frac{6\pi x}{L_1}\right)\cos\left(\frac{\pi z}{H}\right), \\ v(x,y,z,0) = \left(\frac{1}{2}+\frac{y}{2L_2}\right)\sin^2\left(\frac{6\pi x}{L_1}\right)\cos\left(\frac{\pi z}{H}\right) + 0.2\sin^2\left(\frac{4\pi x}{L_1}\right), \\ w(x,y,z,0) = -\frac{H}{\pi}\sin\left(\frac{\pi z}{H}\right)\left(\frac{18\pi}{L_1}\sin^2\left(\frac{6\pi x}{L_1}\right)\cos\left(\frac{6\pi x}{L_1}\right) + \frac{1}{2L_2}\sin^2\left(\frac{6\pi x}{L_1}\right)\right), \\ \phi(x,y,z,0) = 0.01\left(1-\frac{y}{L_2}\right)\left(-\frac{H}{\pi}\cos\left(\frac{\pi z}{H}\right) - \frac{H}{2\pi}\cos\left(\frac{2\pi z}{H}\right)\right)\sin^2\left(\frac{4\pi x}{L_1}\right), \\ \psi(x,y,z,0) = 0.01\left(1-\frac{y}{L_2}\right)\left(\sin\left(\frac{\pi z}{H}\right) + \sin\left(\frac{2\pi z}{H}\right)\right)\sin^2\left(\frac{4\pi x}{L_1}\right). \end{cases} \tag{4.1}$$

We note here that the initial conditions for u_1, u_2, etc., can be easily derived from (4.1), because the functions on the right-hand side of (4.1) are linear in y, and they can be fully decomposed in terms of the hat functions h_1, h_2 and h_3 (see Fig. 2.1). The initial conditions for each mode are then computed by the formulas (3.1) and (3.2). When restricted to the middle half domain, the functions in (4.1) also provide the initial conditions for the simulation on the middle half domain (see Section 4.2).

For the simulation on the domain Ω_0 we prescribe *homogeneous* boundary conditions for the modes $n \geqslant 1$. Specifically, for the subcritical modes, i.e. when $1 \leqslant n \leqslant n_c$,

$$\begin{cases} \xi_n(0,t) = 0, \\ \boldsymbol{v}_n(0,t) = 0, \\ \boldsymbol{\eta}_n(L_1,t) = 0 \end{cases} \tag{4.2}$$

and for the supercritical modes, i.e. when $n > n_c$,

$$\begin{cases} \xi_n(0,t) = 0, \\ \boldsymbol{v}_n(0,t) = 0, \\ \boldsymbol{\eta}_n(0,t) = 0. \end{cases} \tag{4.3}$$

For the zero mode ($n = 0$) we prescribe the *almost homogeneous* boundary conditions:

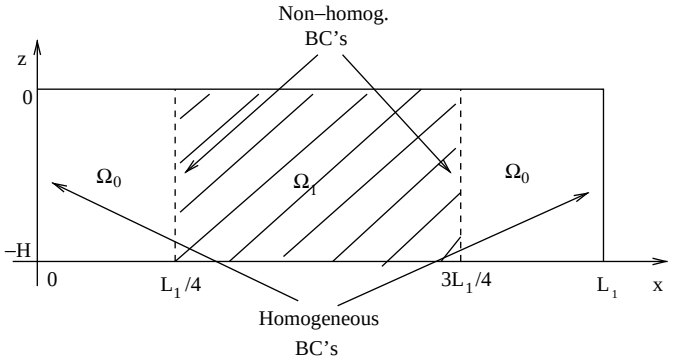

Fig. 4.1. The larger domain Ω_0 and the middle half domain Ω_1.

$$\begin{cases} \boldsymbol{u}_0(0,t) = 0, \\ \boldsymbol{v}_0(0,t) = 0, \\ \phi_0(0,t) = 0, \\ \phi_0(L_1,t) = \phi^r_{0,g}(t), \end{cases} \tag{4.4}$$

where $\phi^r_{0,g}(t)$ provides the "geostrophic" boundary condition for ϕ_0, and is computed by the procedure described in Section 2.5.

Figs. 4.2–4.4 show the initial state of the prognostic unknowns $\boldsymbol{u}$, $\boldsymbol{v}$ and ψ.

Figs. 4.5–4.7 show the state of the prognostic unknowns at the final time $t = T$.

4.2. Simulation on the middle-half domain

Next we do simulation on the middle half domain $\Omega_1 = (L_1/4, 3L_1/4) \times (-H, 0)$ of Ω_0. The boundary values of the unknown function $\boldsymbol{u}$, etc., at $x = L_1/4$ and $3L_1/4$ come from the previous simulation. More specifically, the boundary conditions are, for *the subcritical modes* $(1 \leqslant n \leqslant n_c)$,

$$\begin{cases} \xi_n(L_1/4,t_k) = \xi^l_n(t_k), \\ \boldsymbol{v}_n(L_1/4,t_k) = \boldsymbol{v}^l_n(t_k), \\ \eta_n(3L_1/4,t_k) = \eta^r_n(t_k) \end{cases} \tag{4.5}$$

for *the supercritical modes* $(n > n_c)$,

$$\begin{cases} \xi_n(L_1/4,t_k) = \xi^l_n(t_k), \\ \boldsymbol{v}_n(L_1/4,t_k) = \boldsymbol{v}^l_n(t_k), \\ \eta_n(L_1/4,t_k) = \eta^l_n(t_k) \end{cases} \tag{4.6}$$

and for *the zero mode* $(n = 0)$,

$$\begin{cases} \boldsymbol{u}_0(L_1/4,t_k) = \boldsymbol{u}^l_0(t_k), \\ \boldsymbol{v}_0(L_1/4,t_k) = \boldsymbol{v}^l_0(t_k), \\ \phi_0(L_1/4,t_k) = \phi^l_0(t_k), \\ \phi_0(3L_1/4,t_k) = \phi^r_{0,g}(t_k). \end{cases} \tag{4.7}$$

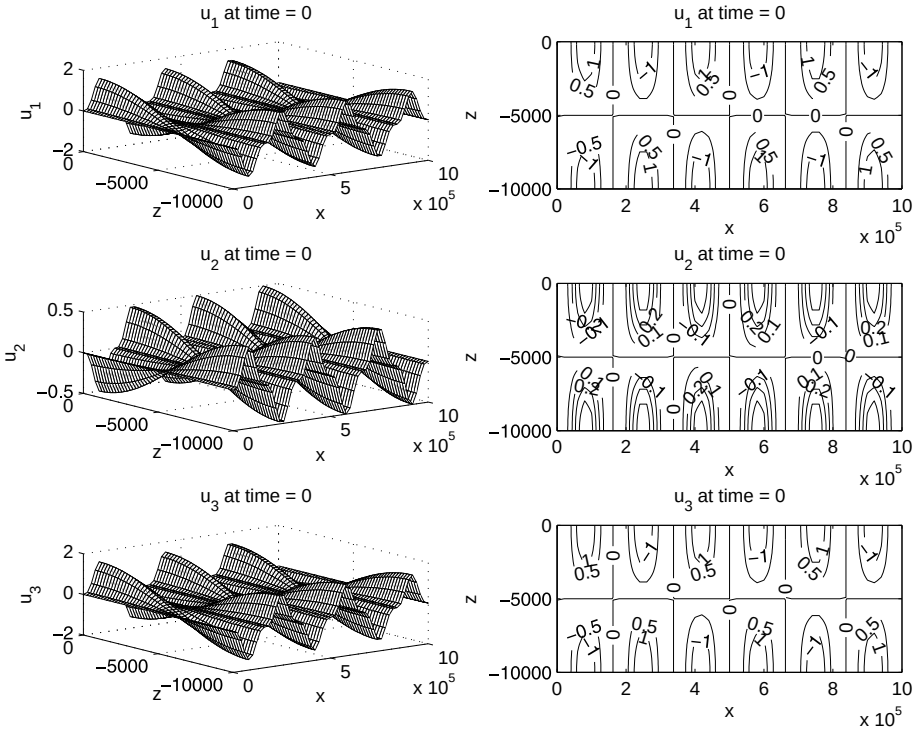

Fig. 4.2. $\boldsymbol{u}$ at $t = 0$ on the larger domain Ω_0.

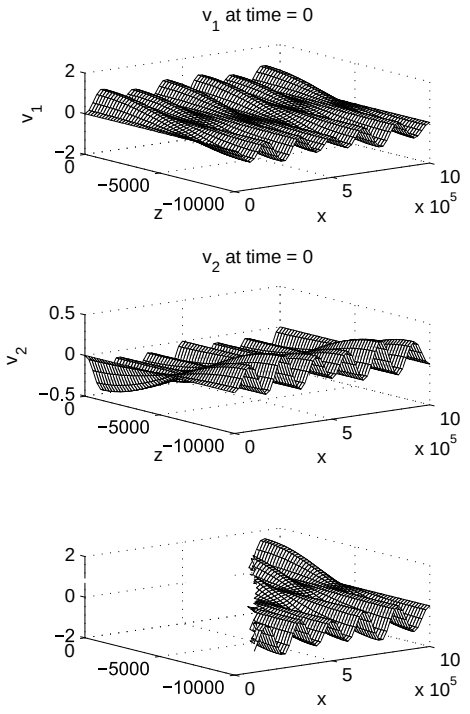

In the above, t_k is the k_{th} time step, $t_k = k\Delta t$. Except for $\boldsymbol{\phi}^r_{0,\text{g}}(t_k)$, all the discrete function values such as $\boldsymbol{\xi}^l_n(t_k)$, or $\boldsymbol{v}^l_n(t_k)$, come from the previous simulation (see Section 4.1); $\boldsymbol{\phi}^r_{0,\text{g}}(t_k)$ is, at each time step, computed from the known quantities by the procedure described in Section 2.5.

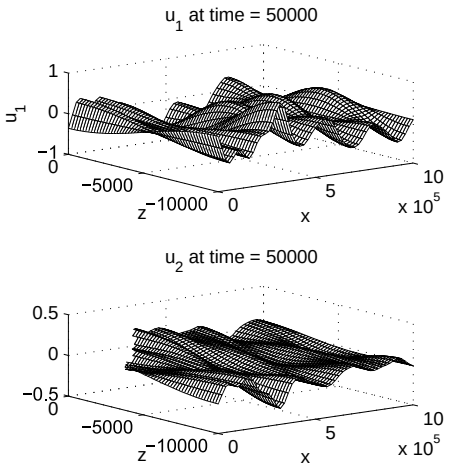

Figs. 4.8–4.10 show the simulation results of the prognostic unknowns $\boldsymbol{u}$, $\boldsymbol{v}$ and $\boldsymbol{\eta}$ in the middle half domain Ω_1 at the final time T.

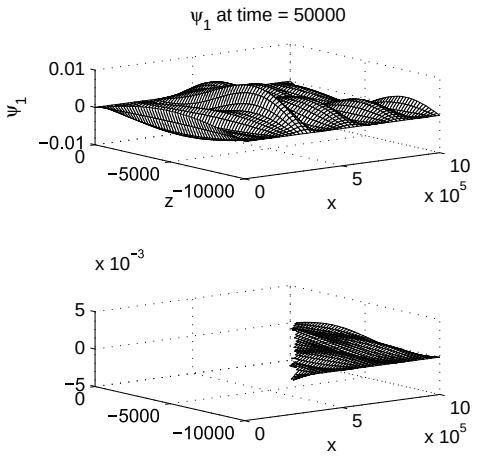
ψ1 at time = 50000
0.01
0
−0.01
ψ1
0
−5000
−10000
z
0
5
10
x
x 10^5

x 10^−3
5
0
−5
0
−5000
−10000
0
5
10
x
x 10^5

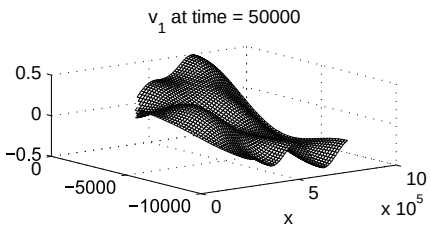
v1 at time = 50000
0.5
0
−0.5
0
−5000
−10000
0
5
10
x 10^5
x

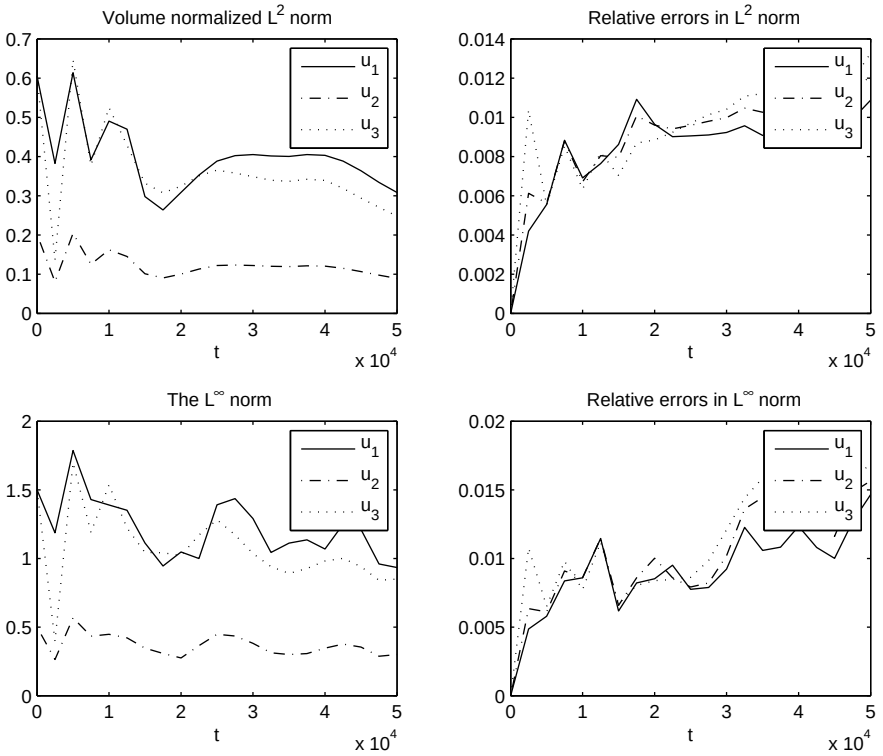

Fig. 4.11. The evolutions of $\boldsymbol{u}$ and of the relative error in volume normalized L^2 norm and in L^∞ norm.

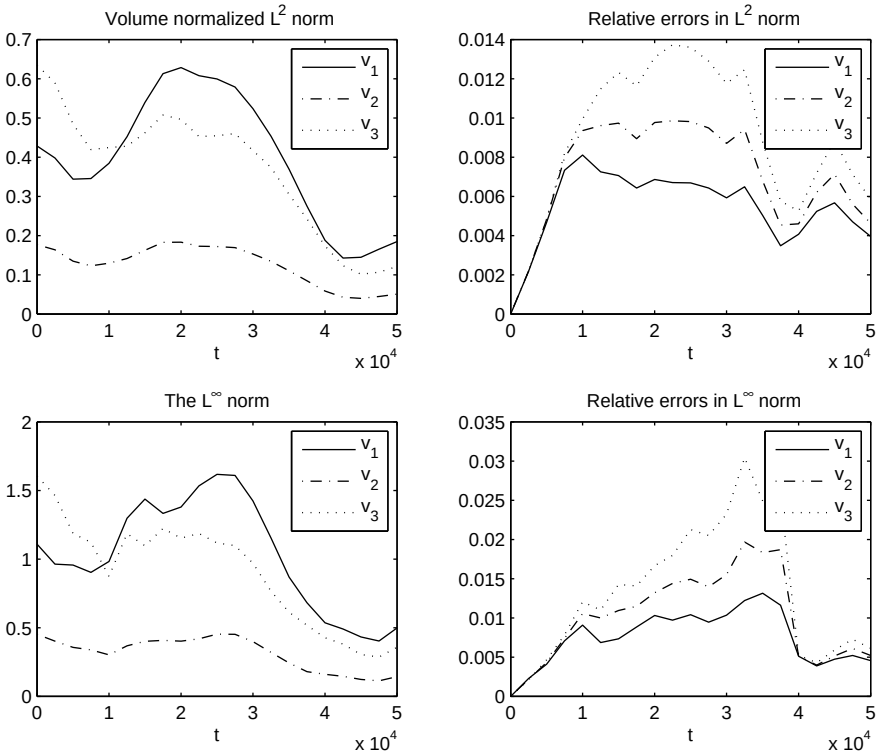

Fig. 4.12. The evolutions of $\boldsymbol{v}$ and of the relative error in volume normalized L^2 norm and in L^∞ norm.

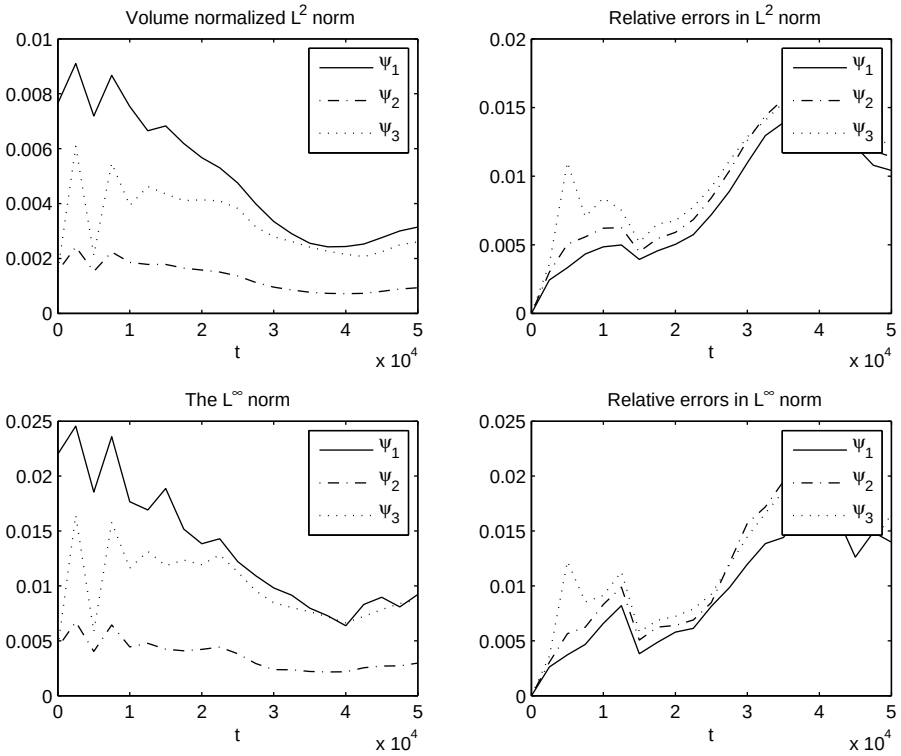

Fig. 4.13. The evolution of ψ and of the relative error in volume normalized L^2 norm and in L^∞ norm.

4.3. Comparisons

In this section we compare the simulation results on the middle half domain Ω_1 (Section 4.2) and the simulation results on the larger domain Ω_0 (Section 4.1) restricted to the middle half domain Ω_1.

Let $\boldsymbol{u}^{\text{ext}}$, $\boldsymbol{v}^{\text{ext}}$, ψ^{ext} be the numerical approximations of the unknown $\boldsymbol{u}$, $\boldsymbol{v}$, ψ on the larger domain Ω_0, respectively, and $\boldsymbol{u}^{\text{int}}$, $\boldsymbol{v}^{\text{int}}$, ψ^{int} be the numerical approximations of the unknown $\boldsymbol{u}$, $\boldsymbol{v}$, ψ on the middle half domain Ω_1, respectively. In Figs. 4.11, 4.12 or 4.13, on the left column, we plot the evolutions of the volume-normalized L^2 norm and the L^∞ norm of $\boldsymbol{u}^{\text{int}}$, $\boldsymbol{v}^{\text{int}}$, ψ^{int} in the middle half domain Ω_1, respectively; and on the right column, we plot the evolutions of the relative errors of $\boldsymbol{u}^{\text{int}}$, $\boldsymbol{v}^{\text{int}}$, ψ^{int} with respect to $\boldsymbol{u}^{\text{ext}}$, $\boldsymbol{v}^{\text{ext}}$, ψ^{ext} in L^2- and $L^\infty-$ norms, respectively, that is, $\|\boldsymbol{u}^{\text{int}} - \boldsymbol{u}^{\text{ext}}|_{\Omega_0}\|_{L^p} / \|\boldsymbol{u}^{\text{int}}\|_{L^p}$, $\|\boldsymbol{v}^{\text{int}} - \boldsymbol{v}^{\text{ext}}|_{\Omega_0}\|_{L^p} / \|\boldsymbol{v}^{\text{int}}\|_{L^p}$, $\|\psi^{\text{int}} - \psi^{\text{ext}}|_{\Omega_0}\|_{L^p} / \|\psi^{\text{int}}\|_{L^p}$, with $p = 2$ and ∞. We note here that the relative errors in both norms are at most of order 10^{-2}, which means that $\boldsymbol{u}^{\text{ext}}$ and $\boldsymbol{u}^{\text{int}}$, $\boldsymbol{v}^{\text{ext}}$ and $\boldsymbol{v}^{\text{int}}$, and ψ^{ext} and ψ^{int} match quite well on the middle half domain Ω_1.

5. Conclusion

In this article we considered the 2.5D inviscid PEs in a limited domain. We recalled the well-posedness results for the linear equations from previous work [3], and presented here the numerical results for the nonlinear equations. Two simulations were performed: the initial one on a larger domain, with homogeneous boundary conditions, and the second one in the middle half domain, using the nonhomogeneous boundary conditions derived from the former calculations. The outcomes of both simulations indicate that the proposed boundary conditions are suitable in this test case for the problems, linear and nonlinear. That the results match very well on the middle half domain demonstrate that the proposed boundary conditions are well suited for simulations in a limited area model (LAM) for which the boundary of the domain is not physical and thus no physical law can provide the boundary conditions that we need, a major difficulty for LAMs highlighted in [24].

Acknowledgement

We thank the anonymous referee for bringing various references to our attention. This work was supported in part by NSF Grant DMS0604235 and by the Research Fund of Indiana University.

Appendix A. Existence and uniqueness result for ϕ_0

We want to discuss the existence and uniqueness of solutions for Eq. (2.36) supplemented with boundary conditions at $x = 0$ and L_1. Without loss of generality we can consider the case of homogeneous boundary conditions and since t is a fixed parameter we do not mention it.

Hence we want to show the existence and uniqueness of the solution ϕ_0 for the equation

$$\begin{cases} \phi_{0xx} + \Lambda^2 \phi_0 = -f\zeta_0, \quad 0 < x < L_1, \\ \phi_0(0) = 0, \quad \phi_0(L_1) = 0. \end{cases} \tag{A.1}$$

We set $\boldsymbol{H} = (L^2(0, L_1))^3$, and denote by A the unbounded operator in $\boldsymbol{H}$, $A = -\mathrm{d}^2/\mathrm{d}x^2$ with domain $D(A) = (H_0^1(0, L_1) \cap H^2(0, L_1))^3$. Since A is invertible, Eq. (A.1) is equivalent to

$$(A - \Lambda^2)\phi_0 = f\zeta_0, \quad \phi_0 \in D(A), \tag{A.2}$$

or

$$(I - A^{-1}\Lambda^2)\phi_0 = A^{-1}f\zeta_0, \quad \phi_0 \in D(A). \tag{A.3}$$

For ζ_0 given in $\boldsymbol{H}$, the existence and uniqueness of the solution for (A.3) follow from the Fredholm alternative; see [20]. Since A^{-1} is compact and Λ is continuous, we only need to show that, for $\zeta_0 = 0$, the unique solution of (A.1) is $\phi_0 = 0$.

Lemma 5.1. The homogeneous equation

$$\phi_{0xx} + \Lambda^2 \phi_0 = 0, \tag{A.4}$$

equipped with the homogeneous boundary conditions $(A.1)_2$, only possesses the zero solution.

Proof 1. Let

$$\sigma_1 = \frac{1}{\sqrt{2}}\begin{pmatrix} 1 \\ 0 \\ -1 \end{pmatrix}, \quad \sigma_2 = \frac{1}{\sqrt{19}}\begin{pmatrix} 3 \\ -1 \\ 3 \end{pmatrix}, \quad \sigma_3 = \frac{1}{\sqrt{38}}\begin{pmatrix} 1 \\ 6 \\ 1 \end{pmatrix}. \tag{A.5}$$

It is easily verified that σ_1, σ_2 and σ_3 form an orthonormal basis of $\mathbb{R}^3$, and that

$$\mathrm{Ker}(\Lambda^2) = \{\sigma_1, \sigma_2\}, \tag{A.6}$$

$$\mathrm{Range}(\Lambda^2) = \{\sigma_2\}, \tag{A.7}$$

$$\Lambda^2 \sigma_3 = \frac{57}{\sqrt{2}L_2^2}\sigma_2. \tag{A.8}$$

We decompose ϕ_0 in terms of this orthonormal basis,

$$\phi_0 = \phi_0^1\sigma_1 + \phi_0^2\sigma_2 + \phi_0^3\sigma_3. \tag{A.9}$$

We insert (A.9) into (A.4), and using (A.6) and (A.8), we find

$$\phi_{0xx}^1\sigma_1 + \left(\phi_{0xx}^2 + \frac{57}{\sqrt{2}L_2^2}\phi_0^3\right)\sigma_2 + \phi_{0xx}^3\sigma_3 = 0. \tag{A.10}$$

Hence we have

$$\begin{cases} \phi_{0xx}^1 = 0, \\ \phi_{0xx}^2 + \frac{57}{\sqrt{2}L_2^2}\phi_0^3 = 0, \\ \phi_{0xx}^3 = 0. \end{cases} \tag{A.11}$$

The boundary conditions $(A.1)_2$ for ϕ_0 imply that

$$\phi_0^i(0) = \phi_0^i(L_1) = 0, \quad \text{for } i = 1, 2, 3. \tag{A.12}$$

We then successively deduces from (A.11) and (A.12) that ϕ_0^1, ϕ_0^3 and ϕ_0^2 vanish.

In conclusion,

Theorem 5.1. For every $\zeta_0 \in \boldsymbol{H}$, (A.1),(A.3) have a unique solution $\phi_0 \in D(A)$.

References

[1] E. Blayo, L. Debreu, Revisiting open boundary conditions from the point of view of characteristic variables, Ocean Model. 9 (2005) 231–252.

[2] C. Cao, E.S. Titi, Global well-posedness of the three-dimensional viscous primitive equations of large scale ocean and atmosphere dynamics, Ann. Math. (2) 166 (1) (2007) 245–267.
[3] Q. Chen, J. Laminie, A. Rousseau, R. Temam, J. Tribbia, A 2.5D Model for the equations of the ocean and the atmosphere, Anal. Appl. 5 (3) (2007) 199–229.
[4] H.C. Davies, A lateral boundary formulation for multi-level prediction models, Quart. J. Roy. Meteor. Soc. 102 (1976) 405–418.
[5] A. Debussche, J. Laminie, E. Zahrouni, A dynamical multi-level scheme for the Burgers equation: wavelet and hierarchical finite element, J. Sci. Comput. 25 (3) (2005) 445–497.
[6] D. Givoli, Nonreflecting boundary conditions, J. Comput. Phys. 94 (1) (1991) 1–29.
[7] G.M. Kobelkov, Existence of a solution 'in the large' for the 3D large-scale ocean dynamics equations, CR Acad. Sci. Paris, Ser. 343 (2006) 283–286.
[8] G.M. Kobelkov, Existence of a solution in the large for ocean dynamics equations, J. Math. Fluid Mech. 9 (4) (2007) 588–610.
[9] J.L. Lions, R. Temam, S. Wang, New Formulations of the primitive equations of the atmosphere and applications, Nonlinearity 5 (1992) 273–288.
[10] J.L. Lions, R. Temam, S. Wang, On the equations of the large-scale ocean, Nonlinearity 5 (1992) 1007–1053.
[11] A. McDonald, A step toward transparent boundary conditions for meteorological models, Mon. Weath. Rev. 130 (2002) 140–151.
[12] A. McDonald, Transparent boundary conditions for the shallow water equations: testing in a nested environment, Mon. Weath. Rev. 131 (2003) 698–705.
[13] A. McDonald, Transparent boundary conditions for baroclinic waves: a study of two elementary systems of equations, Tellus 57A (2005) 171–182.
[14] J. Oliger, A. Sundström, Theoretical and practical aspects of some initial boundary value problems in fluid dynamics, SIAM J. Appl. Math. 35 (3) (1978) 419–446.
[15] J. Pedlosky, Geophysical Fluid Dynamics, second ed., Springer, 1987.
[16] M. Petcu, R. Temam, M. Ziane, Mathematical problems for the primitive equations with viscosity, in: P.G. Ciarlet (Ed.), Handbook of Numerical Analysis Special Issue on Some Mathematical Problems in Geophysical Fluid Dynamics (R. Temam, J. Tribbia, guest eds.), Elsevier, New York, 2007.
[17] A. Rousseau, R. Temam, J. Tribbia, Boundary conditions for an ocean related system with a small parameter, in: G. Chen, G. Gasper, J. Jerome (Eds.), Nonlinear PDEs and Related Analysis Contemporary Mathematics, vol. 371, AMS, Providence, 2005, pp. 231–263.
[18] A. Rousseau, R. Temam, J. Tribbia, Boundary conditions for the 2D linearized PEs of the ocean in the absence of viscosity, Discrete Contin. Dynam. Syst. 13 (2005) 1257–1276.
[19] A. Rousseau, R. Temam, J. Tribbia, Numerical simulations of the inviscid primitive equations in a limited domain, Proceedings of Mathematical Methods for Hydrodynamics, University of Lille, 2005.
[20] W. Rudin, Functional Analysis, second ed., McGraw-Hill, New York, 1991.
[21] R. Temam, J. Tribbia, Open boundary conditions for the primitive and Boussinesq equations, J. Atmos. Sci. 60 (2003) 2647–2660.
[22] R. Temam, M. Ziane, Some mathematical problems in geophysical fluid dynamics, in: S. Friedlander, D. Serre (Eds.), Handbook of Mathematical Fluid Dynamics, vol. 3, North Holland, 2004.
[23] W. Washington, C. Parkinson, An Introduction to Three-dimensional Climate Modelling, second ed., University Science Books, Sausalito, CA, 2005.
[24] T.T. Warner, R.A. Peterson, R.E. Treadon, A tutorial on lateral boundary conditions as a basic and potentially serious limitation to regional numerical weather prediction, Bull. Amer. Meteor. Soc. 78 (11) (1997) 2599–2617.